Investigating the Origin of Enhanced C_{2+} Selectivity in Oxide-/Hydroxide-derived Copper Electrodes during CO_2 Electroreduction

Qiong Lei,[†,¶] Hui Zhu,[†,¶] Kepeng Song,[†] Nini Wei,[§] Lingmei Liu,[†] Daliang Zhang,[#] Jun Yin,[‡] Xinglong Dong,[†,Σ] Kexin Yao,[#] Ning Wang,[†] Xinghua Li,[†,⊥] Bambar Davaasuren,[§] Jianjian Wang,[#] Yu Han*[,†,Σ]

[†] Advanced Membranes and Porous Materials Center, Physical Sciences and Engineering Division, King Abdullah University of Science and Technology (KAUST), Thuwal 23955-6900, Saudi Arabia.

[§] Imaging and Characterization Core Lab, KAUST, Thuwal 23955-6900, Saudi Arabia.

[#] Multi-scale Porous Materials Center, Institute of Advanced Interdisciplinary Studies, & School of Chemistry and Chemical Engineering, Chongqing University, Chongqing 400044, P. R. China.

[‡] Physical Sciences and Engineering Division, KAUST, Thuwal 23955-6900, Saudi Arabia.

[Σ] KAUST Catalysis Center, KAUST, Thuwal 23955-6900, Saudi Arabia.

[⊥]School of Physics, Northwest University, Xi'an 710069, P. R. China.

ABSTRACT: Oxide-/hydroxide-derived copper electrodes exhibit excellent selectivity toward C_{2+} products during electrocatalytic CO_2 reduction reaction (CO_2RR). However, the origin of such enhanced selectivity remains controversial. Here, we prepared two Cu-based electrodes with mixed oxidation states, namely HQ-Cu (containing Cu, Cu_2O, CuO) and AN-Cu (containing Cu, $Cu(OH)_2$). We extracted ultra-thin specimen from the electrodes using a focused ion beam to investigate the distribution and evolution of various Cu species by electron microscopy and electron energy loss spectroscopy. We found that at the steady stage of CO_2RR, the electrodes have all been reduced to Cu^0, regardless of the initial states, suggesting that the high C_{2+} selectivities are not associated with specific oxidation states of Cu. We verified this conclusion by control experiments, in which HQ-Cu and AN-Cu were pretreated to fully reduce oxides/hydroxides to Cu^0, and the pretreated electrodes showed even higher C_{2+} selectivity, compared with their un-pretreated counterparts. We observed that the oxide/hydroxide crystals in HQ-Cu and AN-Cu were fragmented into nano-sized irregular Cu grains under the applied negative potentials. Such a fragmentation process, which is the consequence of an oxidation-reduction cycle and does not occur in electropolished Cu, not only built an intricate network of grain boundaries, but also exposed a variety of high-index facets. These two features greatly facilitated the C-C coupling, thus accounting for the enhanced C_{2+} selectivity. Our work demonstrates that the use of advanced characterization techniques enables investigating the structural and chemical states of electrodes in unprecedented detail, to gain new insights into a widely studied system.

INTRODUCTION

Electrochemical reduction is one of the most appealing methods to convert CO_2 to value-added products, including CO, formic acid or formate, methane, methanol and other multi-carbon oxygenates and hydrocarbons (denote as C_{2+}).[1-7] Among all the reported electrocatalysts for CO_2RR,[8-16] Cu or Cu-based catalyst has drawn the most attention because it can produce deep reduction products (*i.e.*, oxygenates and hydrocarbons) which are more desirable, considering their higher energy density and wider applicability.[4, 17-18] On the mechanism level, such unique performance is attributed to its optimal electronic structure for the rate-limiting CO protonation step, as well as the optimal binding energy for *CO and *COOH intermediates, making the catalyst surface can stabilize *COOH without being poisoned by CO.[19] Meanwhile, the drawback is a moderate binding energy of most reaction intermediates lowers the selectivity toward a certain product.[17]

When electropolished Cu is used as the catalyst, there are 16 products detected after CO_2RR.[20] Methane is the major product, but its faradaic efficiency (FE) decreased quickly after the first two hours from about 50% to 10%.[21] Many strategies have been developed to improve the activity and tune the selectivity of Cu, including surface facet control,[22-27] morphology manipulation,[28-30] single

atom doping,[31] alloying with other metals,[32-33] and deriving from copper oxides or hydroxide,[34-36] etc. Among all the mentioned strategies, special attention has been paid to the oxide-/hydroxide-derived copper electrocatalysts, because their selectivity toward C_{2+} products can generally reach a FE more than 50%.[34-36] However, there is no common understanding on the origin of such excellent performance, and the key oxidation state of Cu is still under debate.[37]

Essentially, the controversy mainly lies on the presence of oxidized Cu phases during the electroreduction of CO_2. Jiang *et al.* reported a FE of 60% for C_{2+} with an electrodeposited Cu_2O(100) electrode.[38] They found there is no oxygen signals can be observed with electron energy loss spectroscopy (EELS) nor energy dispersive X-ray spectroscopy (EDS) on the electrode surface under CO_2RR condition, and the product selectivity owes to the promoted C-C coupling on Cu(100) facet. Similarly, Kim and coworkers found that the chemically deposited $Cu(OH)_2$ nanowires were completely reduced to metallic Cu after a few minutes of electrolysis, which is confirmed by X-ray diffraction (XRD) and electrochemical impedance spectroscopy (EIS), and they gave the credit of 38% FE for C_{2+} to systemically modified mesostructure.[39] On the other hand, several groups have evidenced the presence of oxygen species on the surface of oxide-/hydroxide-derived copper electrodes under CO_2RR conditions, and related it to the enhanced C_{2+} selectivity.[34-36, 40-43] For example, Mistry *et al.* used scanning transmission electron microscopy (STEM) equipped with EDS, operando X-ray absorption fine structure (XAFS) and high resolution transmission electron microscopy (HRTEM) to prove that the surface Cu^{1+} species in their plasma treated Cu foil is stable during CO_2RR, and the superb selectivity on ethylene (FE 60%) relies on the existence of Cu^{1+}.[36] Additionally, grazing incidence XRD (GI-XRD), X-ray photoelectron spectroscopy (XPS), and X-ray absorption near edge structure (XANES) were involved to evidence the stability of $Cu(OH)_2$ and Cu_2O in an anodized Cu electrocatalyst under CO_2RR conditions according to Lee's work.[34] They claimed the high FE of ethylene (~ 38%) and long catalytic lifetime (~ 40 h) to be a result of mixed Cu oxidation states (Cu, Cu_2O, and $Cu(OH)_2$). To end this controversy and facilitate the mechanism study on the origin of enhanced selectivity toward C_{2+} products of oxide-/hydroxide-derived Cu catalysts, it is of great importance to determine the oxidation states of Cu species and their spatial distribution on the electrode during CO_2RR.

In this work, we have prepared two Cu-based electrodes with mixed oxidation states: one containing Cu, Cu_2O, and CuO via a heat-quench process (HQ-Cu), and the other one containing Cu and $Cu(OH)_2$ via anodization (AN-Cu). They were submitted directly or after an electro-reduction pretreatment to CO_2RR and characterized along the process. Focused ion beam (FIB) was used to extract ultra-thin (~ 100 nm) lamella from the electrode, allowing the analysis on the distribution and evolution of different Cu oxidation states on the electrode cross-section using TEM and EELS. During FIB process, carbon precursors were used to react with the electron beam to deposit the first protection layer onto the sample surface and a focused Gallium ion beam was applied to cut and mill the specimen. Under the FIB conditions, carbon precursors and Gallium ions do not react with Cu, Cu_2O, CuO, or $Cu(OH)_2$, and therefore do not affect the oxidation states of Cu. Our results support the argument that metallic Cu is the actual active species and indicate that the starting oxidation state of oxidized Cu, mixed or pure Cu^0, would hardly affect the enhanced selectivity toward C_{2+} products. HRTEM image and selected area electron diffraction (SAED) pattern revealed that the initial micron-sized oxide crystals in HQ-Cu were fragmented into nano-sized Cu grains under the negative potential during electro-reduction pretreatment and CO_2RR. Using a recently developed image processing method, we were able to identify individual Cu grains and their boundaries from the HRTEM images. The results show that these Cu grains are 5-15 nm in size, irregular in shape, exposing a large number of various high-index facets. The crystal fragmentation was only observed in oxide-/hydroxide-derived Cu and not in electropolished Cu, indicating that an oxidation-reduction cycle is its prerequisite. On the basis of the correspondence between "crystal fragmentation" and the high C_{2+} selectivity, we conclude that the increased grain boundaries and high-index facets generated during fragmentation process are the origin of the observed high C_{2+} selectivity of oxide-/hydroxide-derived Cu electrodes.

RESULTS AND DISCUSSIONS

Electrode Preparation and Characterization. Both Cu oxide-/hydroxide-containing electrodes were prepared from electropolished Cu. SEM image indicates a flat surface of the electropolished Cu substrate (Figure 1a), and the XRD pattern clearly shows three sharp intensive peaks at 43.3°, 50.4° and 74.1° that correspond to the (111), (200) and (220) reflections of Cu (PDF#70-3039) (Figure 1d). To prepare the oxide-containing electrode, or HQ-Cu, electropolished Cu was heated in a tube furnace at 1100°C for 10 sec, and immediately quenched in air. This process results in the generation of sponge-like surface on top of Cu substrate (Figure 1b). Apart from the three sharp Cu peaks, five broad peaks at 29.3°, 36.2°, 42.1°, 60.9°, and 72.7° in the XRD pattern of HQ-Cu can be well indexed to the (110), (111), (200), (220) and (311) planes of Cu_2O (PDF#05-0667) (Figure 1d). In addition, there is one weak peak at 38.8°, which could possibly be assigned to CuO. To further confirm the origin of this peak, we consulted Cu 2*p* of XPS, and it provided Cu^{2+} satellites at 962.1 eV and 943.6 eV to evidence the presence of CuO (Figure S1). For the hydroxide-containing electrode, or AN-Cu, electropolished Cu was anodized in 3.0 M potassium hydroxide aqueous electrolyte at a constant current of 10 $mA{\cdot}cm^{-2}$ for 60 sec. The produced electrode has a nanowire surface morphology (Figure 1c), and its XRD pattern perfectly matches with $Cu(OH)_2$ (PDF#80-0656) and Cu (PDF#70-3039) (Figure 1d), indicating the formation of

hydroxide on the Cu substrate. In other words, we have produced two electrodes that consist of mixed Cu oxidation states: the first one is HQ-Cu, containing Cu, Cu_2O and CuO; and the second one is AN-Cu, containing Cu and $Cu(OH)_2$.

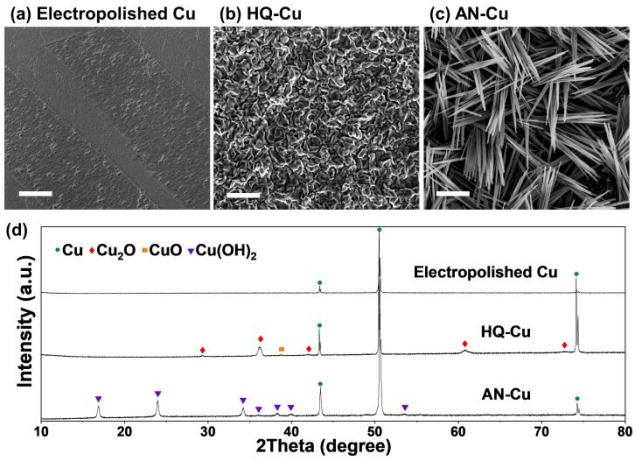

Figure 1. SEM images of (a) electropolished Cu, (b) HQ-Cu, and (c) AN-Cu, in which the scale bars all represent 2 μm; (d) indexed XRD patterns of these three electrodes.

CO_2RR performance. As-prepared HQ-Cu and AN-Cu electrodes were both submitted to CO_2RR directly at different potentials to evaluate their catalytic performance. In comparison with the pure Cu electrode (an electropolished Cu foil), HQ-Cu and AN-Cu have effectively suppressed the CH_4 production at more negative potentials (< -1.1 V *vs* RHE) (Figure 2a), and greatly improved the selectivity toward C_{2+} products at all tested potentials (Figure 2b). The highest FE for C_{2+} of CO_2RR with HQ-Cu can reach 68.2% at a potential of -1.05 V *vs* RHE, while that of CO_2RR with AN-Cu is 62.3% at -1.03 V *vs* RHE. The main C_{2+} products include C_2H_4, C_2H_5OH, C_2H_5CHO, CH_3CHO, n-C_3H_7OH, and CH_3COO^- (sequenced by decreasing FE), and detailed product distribution has been summarized in Figure S2. This result is consistent with other reported works on oxide-/hydroxide-derived Cu that increased C_{2+} selectivity has been observed.[34-35, 44-47] Since C–C coupling is the key step to form C_{2+} products and it directly consume CO* intermediates,[48] decreased CO production can be expected at C_{2+}-favored potentials (< -0.9 V *vs* RHE) (Figure 2c). In addition, H_2 formation has been suppressed as CO_2RR is apparently favored over water splitting on oxide-/hydroxide-derived Cu electrodes at raised cathodic potentials (< -0.8 V *vs* RHE) (Figure 2d). At their optimum potential for C_{2+} production, the partial current densities for C_{2+} of HQ-Cu and AN-Cu are approximately 50 and 64 times that of electropolished Cu, respectively (Figure 2e). By prolonging the reaction time, we found the C_{2+} selectivities of HQ-Cu and AN-Cu can both be extended to more than seven hours (Figure 2f). In short, comparing with electropolished Cu, oxide-/hydroxide-derived Cu electrodes can not only extensively enhance the C_{2+} selectivity, but also greatly improve the catalytic activity and stability.

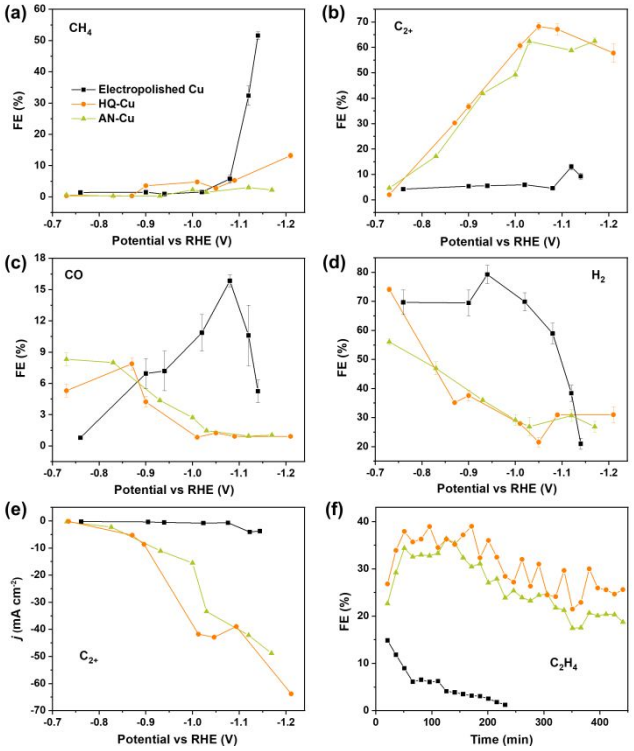

Figure 2. Comparison on faradaic efficiency (FE) of (a) CH_4, (b) C_{2+}, (c) CO and (d) H_2 for CO_2RR with electropolished Cu, HQ-Cu and AN-Cu at different potentials. (e) Comparison on partial current density of C_{2+} for CO_2RR with these three electrodes. Data has been normalized by electrochemically active surface area (ECSA). (f) Catalytic lifetime test on CO_2RR at -1.2 V *vs* RHE with these three electrodes. All CO_2RR were conducted in CO_2-saturated 0.1 M $KHCO_3$.

Evolution of electrode species during CO_2RR. Although the improved C_{2+} selectivity of oxide-/hydroxide-derived Cu electrode has been well noted, there is no consensus on the origin of such change. In theory, bulk Cu oxide/hydroxide species should be reduced to metallic Cu at the negative potentials of CO_2RR, but the presence of oxygen in electrode surface is still under debate.[37] To study the evolution of electrode species under CO_2RR conditions, we used EELS to depict different Cu oxidation states of HQ-Cu before and after reaction. FIB technique was utilized to cut a thin slice out of the electrode, which allowed us to investigate the distribution and evolution of different Cu oxidation states along its cross-section. Firstly, we studied HQ-Cu and found that three types of Cu species (Cu^0, Cu^{1+}, Cu^{2+}) coexisted but resided in separate layers (Figure 3a), which is in line with the previous reports on Cu oxidation mechanism.[49-50] Specifically, Cu^{2+} is present on the top surface, forming a thin, rugged and discontinuous layer (0 to 200 nm in thickness). A continuous layer of Cu^{1+} is sandwiched between the top surface of Cu^{2+} and the substrate of Cu^0 with thickness of ~ 300-1000 nm. EELS spectra extracted from these three layers perfectly match with the standard spectra for Cu,

Cu_2O, and CuO (Figures S3a,b).[51] This result agrees well with our XRD and XPS analysis described above. Although the trace amount of CuO on the outermost surface is difficult to be detected by XRD, it has been clearly observed by XPS and electron microscopy. Taken together, these results show that in HQ-Cu electrode, the oxidation degree increases from the bulk to the surface, with the overall thickness of the oxidation layers at several hundreds of nanometers. We note that in the FIB-fabricated specimen, there is often a crack at the interface of the oxide layer and the substrate (Figure 3, indicated by white arrows), which might be a result of different tension between Cu_2O and Cu crystals, and sometimes further stretched by FIB operation.

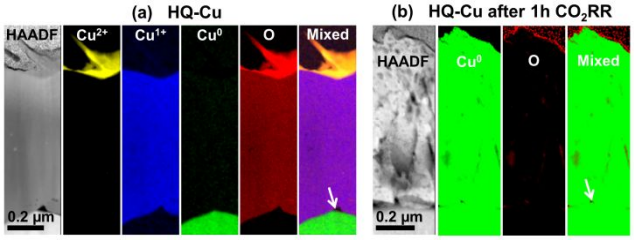

Figure 3. High-angle annular dark field (HAADF) STEM image and the corresponding EELS mapping on different Cu oxidation states and oxygen of the FIB-fabricated specimen that corresponds to the cross-section of (a) HQ-Cu; and (b) HQ-Cu after 1 h of CO_2RR at 1.05 V *vs* RHE in CO_2-saturated 0.1 M $KHCO_3$.

To identify the active Cu species for the enhanced C_{2+} selectivity, we submitted HQ-Cu to CO_2RR at -1.05 V *vs* RHE for 1 h, allowing the catalytic performance to reach the steady stage, and then terminated the reaction to ex-situ investigate the Cu oxidation states with XRD and FIB-TEM/EELS. The XRD pattern showed that all reflections associated with Cu_2O and CuO disappeared after 1 h of CO_2RR reaction (Figure S4). Accordingly, there was only metallic Cu (Cu^0) detected by EELS throughout the entire cross-section of the electrode (Figure 3b). The EELS spectra collected from the upper layer, where Cu_2O and CuO were present in the initial HQ-Cu electrode, and the lower Cu substrate are identical, and no oxygen peak has been observed in both areas (Figures S3c,d). Trace amount of oxygen was detected by EELS at the surfaces contacting with the Pt/C FIB-protection layer and along the crack between the initial Cu_2O layer and the Cu substrate (Figure 3b), which we believe is due to the inevitable exposure to the air during the sample-transfer processes in FIB and TEM imaging. In fact, the oxygen contamination issue has been aware of in the literature when the reduced Cu electrodes are ex-situ characterized, and this issue makes it difficult to completely rule out the presence of residual unreduced Cu oxide species.[52-53] Although this issue remains in this study, our characterization using analytical electron microscopy provides sufficiently high spatial resolution to reveal that the very little amount of oxygen resides only at the two surfaces of the oxidized/reduced layer. This observation suggests that the oxygen is from contamination instead of unreduced Cu oxides, because the latter, if it exists, should not reside in the interior of the electrode (the cracked interface), given that the electro-reduction of the electrode takes place from the substrate outwards.

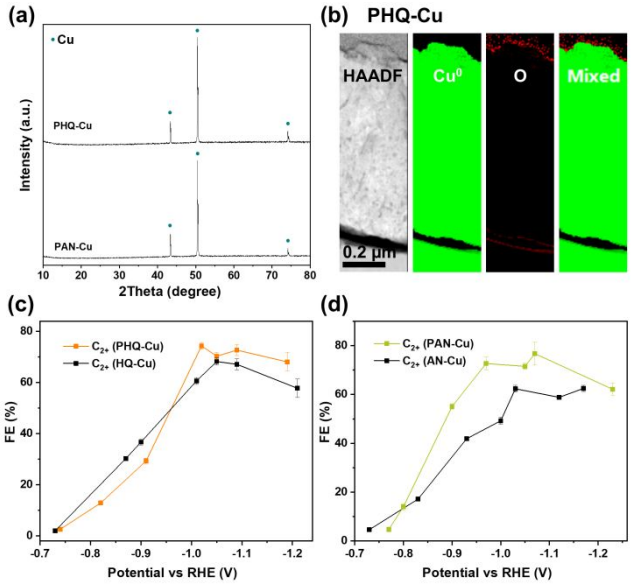

Figure 4. (a) Indexed XRD patterns of PHQ-Cu and PAN-Cu; (b) HAADF-STEM image and the corresponding EELS mapping on different Cu oxidation states and oxygen of the FIB-fabricated specimen that corresponds to the cross-section of PHQ-Cu; FE comparison between (c) HQ-Cu and PHQ-Cu, and (d) AN-Cu and PAN-Cu. Detailed product distributions have been summarized in Figures S2 and S6. All CO_2RR were conducted in CO_2-saturated 0.1 M $KHCO_3$.

Pretreatment by electroreduction. Our characterization data suggests that the observed high C_{2+} selectivities are associated with metallic Cu rather than Cu oxides. This is consistent with the reported in situ measurements that have demonstrated the reduction of Cu oxides is prior to the reduction of CO_2, including Cu K-edge X-ray absorption spectroscopy (XAS),[54] GI-XRD,[37] and Raman spectroscopy[55]. To consolidate this conclusion, we performed a harsh electro-pretreatment on the HQ-Cu within the same electrolytic cell, in order to ensure the full reduction of Cu oxides to metallic Cu prior to the CO_2RR reaction. To avoid CO_2RR product accumulation during this process, we applied a highly negative potential for shortened time, and the pretreated electrode is denoted as PHQ-Cu. Specifically, -5.0 V *vs* Ag/AgCl was used for 10 sec. The cathodic current of prolonged pretreatment was also recorded in time, indicating that the current reached a steady state within the first 5 sec and 10 sec at this potential is enough to reduce Cu oxides to Cu^0 (Figure S5). The XRD pattern collected after the electro-reduction pretreatment also indicates the reduction of Cu_2O and CuO to metallic Cu (Figure 4a). It was further confirmed by the results of FIB-EELS analysis performed in the same way as described above for HQ-Cu, which shows only metallic Cu throughout the entire cross-section of the PHQ-Cu electrode (Figure 4b). The EELS spectra collected from the upper oxidized/reduced layer and the lower Cu substrate

are identical, and no oxygen peak has been observed in both areas (Figures S3e,f). In other words, PHQ-Cu is an electrode containing pure Cu^0.

CO_2RR performance of PHQ-Cu has been evaluated at different potentials, and its selectivity toward C_{2+} products is even slightly higher than that of HQ-Cu at higher cathodic potentials (Figure 4c). The highest FE for C_{2+} can reach 72.7% at -1.09 V *vs* RHE. This result supports our conclusion that the observed high selectivity toward C_{2+} products is only associated with pure metallic Cu, rather than any Cu oxides. In addition, exactly same results have been obtained when we performed the electro-reduction pretreatment (-5.0 V *vs* Ag/AgCl for 10 min) on AN-Cu. That is, the AN-Cu has been fully reduced to metallic Cu (Figures 4a, S6a-c), and the obtained electrode is denoted as PAN-Cu. Compared with the hydroxide-containing electrode (AN-Cu), the pretreated one (PAN-Cu) exhibited further enhanced C_{2+} selectivity, and the highest FE can reach 76.73% at -1.07 V *vs* RHE (Figure 4d). In other words, the starting oxidation state of oxidized Cu precursors plays a minor role in determining the selectivity toward C_{2+} products, because they will all be reduced to Cu^0 at the negative potentials of CO_2RR. This is in line with the result from Eilert's observations that the ethylene selectivities are similar between $CuCO_3{\cdot}Cu(OH)_2$ and Cu_2O.[54]

In a separate control experiment, we conducted the same electro-reduction pretreatment on a pure Cu electrode (an electropolished Cu foil), and found that the pretreatment did not change its CO_2RR activity or enhance its C_{2+} selectivity (Figure S7). This result suggests that such an electro-reduction pretreatment alone would not obviously change the catalytic selectivity of the Cu-based electrodes for CO_2RR, whereas the enhanced C_{2+} selectivity of oxide-/hydroxide-derived Cu electrode is a consequence of an oxidation-reduction cycle.

Crystal Fragmentation at Negative Potential. The above findings inspired us to study the common features of Cu electrodes with high C_{2+} selectivity, such as HQ-Cu, PHQ-Cu, AN-Cu and PAN-Cu, and how they distinguish from those with low C_{2+} selectivity, such as electropolished Cu. For this purpose, we maximized the utilization of FIB-TEM and visualized the changes on oxide-/hydroxide-derived Cu crystals under the negative potential of electro-reduction pretreatment or CO_2RR. Firstly, we studied the as-prepared HQ-Cu electrode. The previous assignment of the successive layers ($Cu/Cu_2O/CuO$) in HQ-Cu based on EELS has been confirmed by SAED (Figure 5a). The SAED analysis also indicated that the CuO layer is very thin and discontinuous; the Cu_2O layer consists of large grains with dimensions of ~ 1 μm; the Cu substrate layer consists of even larger grains, whereas the exact grain sizes cannot be determined because there is only one grain boundary observed in the FIB-fabricated specimen. In brief, the three layers follow the order: Cu > Cu_2O > CuO, in terms of grain size. These results demonstrate that the heat-quench process leads to the generation of oxide layers on the surface of Cu foil, with the grain sizes decreasing as the oxidation degree increases.

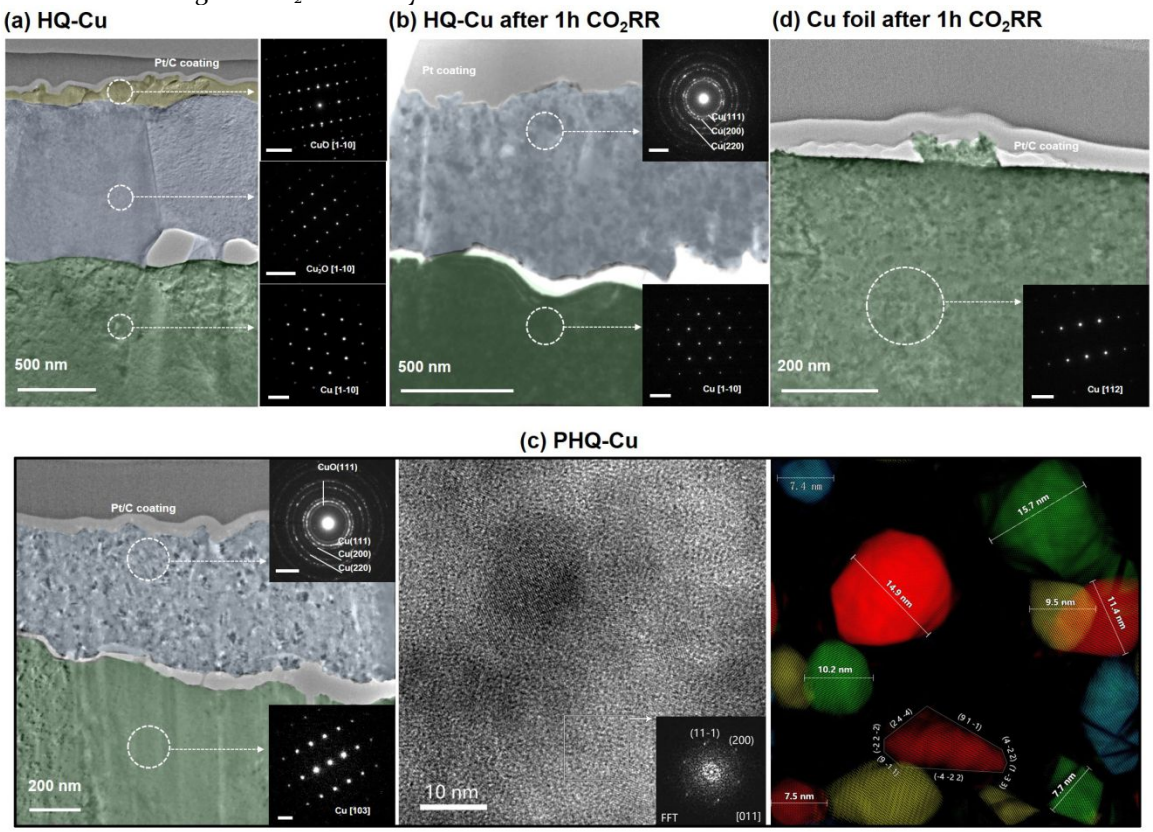

Figure 5. TEM images of FIB-fabricated specimen from different electrodes: (a) HQ-Cu, (b) HQ-Cu after 1h of CO_2RR, (c) PHQ-Cu, and (d) electropolished Cu foil after 1 h of CO_2RR. Each dashed circle represents a selected area with a diameter of ~ 160 nm;

the insets are the corresponding SAED patterns, in which the scale bars all represent 5 1/nm. In (c), the middle panel shows a typical HRTEM image of the oxide-derived layer in PHQ-Cu, acquired from the selected area in the left panel; the right panel shows some Cu grains identified from the HRTEM image using a self-developed image processing software, among which one Cu grain is determined to be oriented along [011] zone axis and its exposed surfaces are all indexed and labelled. We note that there is a dim diffraction ring in the upper SAED pattern in (c), which can be assigned to the (111) reflection of CuO; the generation of CuO in the reduced Cu layer is likely due to unavoidable exposure to the air during the sample transfer processes in FIB and TEM imaging. In the cross section TEM images, the oxide (or oxide-derived) layer and Cu substrate sections are artificially colored in light blue and light green, respectively, for clarity.

Secondly, we investigated two electrodes that had undergone electro-reduction processes, namely HQ-Cu after 1h of CO_2RR and PHQ-Cu, using the same characterization method. The SAED results showed that, in both cases, the oxide layers were fully reduced to metallic Cu (Figures 5b,c), which is consistent with the EELS analysis of oxidation states (Figures 3b and 4b). Remarkably, unlike the as-prepared HQ-Cu electrode in which the oxide layers show single-crystalline diffraction patterns (Figure 5a), these two electrodes show polycrystalline diffraction rings at their oxidized/reduced layers (Figures 5b & 5c). As the selected area for diffraction is ~ 160 nm in diameter, the observed polycrystalline diffraction rings must originate from much smaller, randomly oriented grains. The single-to-polycrystalline evolution implies that the initial micron-sized Cu_2O/CuO grains are fragmented into nano-sized Cu grains during the CO_2RR or electro-reduction pretreatment. The generation of nano-sized Cu grains as a consequence of "fragmentation" has been confirmed by HRTEM imaging. The middle panel in Figure 5c shows a typical HRTEM image acquired from a FIB-fabricated specimen of PHQ-Cu, in which randomly oriented, overlapping lattice fringes are observed. Using a self-developed image processing method based on modified inverse Fourier transform, we are able to isolate each individual grains from the raw image, and thus identify their exact sizes and shapes (Figure 5c; right panel). The results show that Cu grains have irregular shapes and small sizes, ranging from 5 to 15 nm. Although it is impossible to determine the exposed facets of each grains due to their random orientations (most grains show only one set of lattice fringes in the image), we can occasionally find a grain oriented along a zone axis so that we can determine the indexes of some exposed surfaces (edges or facets). One example is outlined in the figure, which is oriented along the [011] zone axis, exposing a number of high-index surfaces including (91-1), (4-22), (1-33), (-4-22), (9-11), (-22-2) and (24-4) (Figure 5c; right panel). We performed HRTEM study for HQ-Cu after 1 h of CO_2RR as well, and obtained similar results (Figure S8). Taken together, these results demonstrate that under the negative potential of both electro-reduction pretreatment and CO_2RR, the oxide crystals in HQ-Cu were fragmented into small irregular Cu grains with many high-index facets exposed. Note that the Cu substrate layer remains single crystalline (i.e., consisting of large grains) in both cases (Figures 5b & 5c). In addition, SEM and TEM characterizations indicate that the spongy HQ-Cu surface (Figure S9a) forms cracks and porous structures under the negative potentials of CO_2RR (Figure S9b) or electrochemical pretreatment (Figure S9c), which is likely associated with crystal fragmentation, or a result of the gas generation (both CO_2RR and HER) under highly negative potential. Such morphological changes slightly increased the electrode surface roughness according to our ECSA analysis (Figure S10 and Table S1). Although we did not characterize AN-Cu as in detail as HQ-Cu, we believe the same conclusion also holds for hydroxide-derived electrodes, because when we characterized the PAN-Cu electrode with the same FIB-TEM technique, similar results has been obtained. That is, the upper hydroxide-derived layer was fully reduced to metallic Cu, and fragmented into nano-sized irregular grains (Figure S11).

Finally, we applied -1.05 V *vs* RHE to an electropolished Cu electrode for 1 h under CO_2RR conditions, and then characterized it with FIB-TEM as described above for other samples. We found that the electrode retained large grain sizes without being fragmented, during the CO_2RR process, as evidenced by the single-crystalline diffraction pattern (Figure 5d). Based on these findings, we conclude that the fragmentation process under the negative potential of both electro-reduction pretreatment and CO_2RR is the consequence of an oxidation-reduction cycle, and therefore does not occur in electropolished Cu.

Given that all Cu electrodes with high C_{2+} selectivity share the common feature of fragmentation and those with low C_{2+} selectivity do not possess this feature, a strong connection can be built between the crystal fragmentations with the improved selectivity toward C_{2+} products. In fact, the fragmentation process can enhance C_{2+} production during CO_2RR in two ways. On one hand, it formed an intricate network of grain boundaries surface terminations, where highly active sites are enriched and facilitating CO binding. The improved CO binding can hold CO* longer, not only increasing the chance for two CO* intermediates to be coupled to generate C_{2+} products, but also limiting the access of H_2O molecules to the active sites and therefore suppressing H_2 evolution.[56-60] Additionally, grain boundaries effect was also reported to be responsible for the improved CO_2 reduction activity at lower overpotentials.[61] On the other hand, such crystal fragmentation provides enormous opportunities for high-index facet exposure, such as (91-1) and (-4-22) (Figure 5c; right panel). The high-index [n(100) × (111)] surfaces have been reported to significantly promote C_2H_4 formation while suppressing CH_4 generation, which can explain the similar selectivity ratio of C_2H_4/CH_4 between PHQ-Cu and Cu (911) single crystal surface[23]. Obviously, different negative potentials and time would vary the fragmentation results. Especially for the short-term pretreatment at highly negative potentials, facets with relatively higher

energy would have higher chance to be preserved after exposure. This can probably explain the slightly higher FE for C_{2+} of PHQ-Cu than that of HQ-Cu. Hahn et al. have investigated the CO_2RR performance of Cu(111), (100), and (751) single crystal surface and found the selectivity toward C_2H_4 over CH_4 is potential-dependent.[22] Taking Cu(100) as an example, C_2H_4 production dominates over CH_4 at lower potentials, and the latter reverse the situation at more negative potentials (e.g., -1.10 V *vs* RHE). While in our case, the selectivity toward C_2H_4 over CH_4 is consistent at all tested potentials ranging from -0.65 to -1.2 V *vs* RHE. In this light, the enhanced selectivity toward C_{2+} products of our HQ-Cu and PHQ-Cu electrodes should be a result of the combination of increased grain boundaries and high-index facets exposed during fragmentation under the negative potential of electro-reduction pretreatment and CO_2RR.

As we were finalizing this manuscript, we noticed a new publication by Hwang et al., which reported that fragmentation of Cu_2O nanoparticles under CO_2RR conditions enhances C-C coupling and therefore boosts C_2H_4 selectivity.[35] These two works coincide in main conclusions. In their report, the FE for C_2H_4 climbed to the plateau after six hours reaction, whereas our catalysts provide the highest FE for C_2H_4 within the first hour (Figure 2f). This difference is possibly due to the very different sizes of initial Cu_2O crystals in the two cases (~ 1 μm *vs* 20 nm): smaller crystals require longer time to get further fragmented under the same negative potential of CO_2RR.

CONCLUSION

In summary, we have prepared two Cu-based electrodes with mixed oxidation states, including HQ-Cu (containing Cu, Cu_2O, CuO), and AN-Cu (containing Cu, $Cu(OH)_2$). Comparing with electropolished Cu, they were found to provide similarly enhanced selectivities for C_{2+} products. FIB-TEM/EELS was used to characterize the distribution and evolution of various Cu species. We found that HQ-Cu electrode was fully reduced to metallic Cu at the steady stage of CO_2RR, suggesting that the observed high C_{2+} selectivities do not depend on specific oxidation states of Cu. In addition, an electro-reduction pretreatment was performed on these two electrodes under harsh conditions to ensure full reduction to Cu^0 before submitted to CO_2RR. The pretreated electrodes exhibited even slightly higher selectivity toward C_{2+} products, further confirming the key catalytic role of Cu^0 and the negligible significance of starting oxidation state of oxidized Cu. Furthermore, we found that the oxide crystals in HQ-Cu and the hydroxide crystals in AN-Cu were all reduced and fragmented into small irregular Cu grains under the negative potential of electro-reduction pretreatment or CO_2RR, while no fragmentation has been observed in electropolished Cu after CO_2RR. Based on these findings, we conclude that such fragmentation is the consequence of an oxidation-reduction cycle, and accounts for the enhanced C_{2+} selectivity of oxide-/hydroxide-derived Cu electrodes, because it greatly facilitates C-C coupling with numbers of grain boundaries and high-index facets. Our work provides new insights into the roles of crystal fragmentation in determining the product selectivity of oxide/hydroxide-derived Cu electrodes during CO_2RR, and should inspire more highly selective electrocatalysts to be developed.

EXPERIMENTAL SECTION

Electrode Preparation. All Cu foils (Alfa Aesar, 0.127mm thickness, 99.9%) were first cleaned in ethanol (VWR, ACS reagent grade) and Milli-Q water (18.2 $M\Omega \cdot cm^{-1}$) under sonication for 10 min each, then electropolished in 85% phosphoric acid (Scharlau, 85% in water) at 3.0 V versus another Cu foil for 5 min. The obtained electropolished Cu was used as-prepared, or after an oxidation process.

The Cu-based electrode with mixed oxidation states was prepared via a successive heat and quench method (denote as HQ-Cu). Specifically, electropolished Cu was heated in a tube furnace (MTI, GSL-1700X) at the desired temperature of 1100°C for 10 sec, and quenched in air right after the allotted time.

Anodized Cu electrode (denote as AN-Cu) was fabricated in a modified method.[34] The electropolished Cu were oxidized in 3.0 M potassium hydroxide (Sigma-Aldrich, 85%) aqueous electrolyte for 60 sec at a constant current of 10 $mA \cdot cm^{-2}$ to form $Cu(OH)_2$ nanowires.

Electroreduction of CO_2. All electro-pretreatment and catalytic measurements were performed on CHI 760e workstation in a commercial H-type gas-tight three-electrode cell. Nafion 117 membrane (Fuel Cell Store) was used to separate the cathode and anode compartments. Platinum foil and Ag/AgCl electrode filled with saturated potassium chloride solution (Ida, R0303) were employed as the counter and reference electrode, respectively. All potentials measured against Ag/AgCl were converted to the reversible hydrogen electrode (RHE) scale in this work using E (*vs* RHE) = E (*vs* Ag/AgCl) + 0.197 V + 0.0591 × pH. 0.1 M potassium bicarbonate (Honeywell, 99.5-101.0% (acidimetric)) aqueous solution saturated with CO_2 (Air Liquide, 99.995%) was the electrolyte, and the pH value was measured to be 6.8 by Orion 5 star benchtop multiparameter (Thermo Scientific).

Geometric dimensions of all electrodes were controlled to be 1 × 6 mm^2. The electro-pretreatment is to apply a highly negative bias potential of –5.0 V *vs* Ag/AgCl for 10 sec on HQ-Cu, or for 10 min on AN-Cu, prior to CO_2RR within the same cell. During CO_2RR, 5.0 standard cubic centimeters per minute (sccm, monitored by Cole-Parmer Scientific mass flow controller) of CO_2 was continuously purged into the system and the gas products were routed into an online gas chromatography (GC, Kechuang GC2002).

Product Analysis. All gas products were analyzed by the online GC, which is equipped with one thermal conductivity detector (TCD) to detect H_2 and two flame ionization detectors (FID) to detect hydrocarbons. Before

the second FID, a methanizer (Kechuang) is installed for the detection of CO. Quantification of gaseous products was determined using calibration curves from standard gases.

All liquid products were quantified by 1D ^{1}H NMR (Bruker, 600 MHz). Standard curves were made using purchased chemicals over the concentration range of interest with 1.67 parts per million (ppm) dimethyl sulfoxide (DMSO, Sigma-Aldrich, 99.9%) as the internal standard in 0.1 M $KHCO_3$. The water peak was suppressed by a presaturation sequence. NMR parameters used were identical between collected spectra to make standard curves and in the subsequent quantification of CO_2RR products in the electrolyte. FE could be calculated as follows:

$$FE = \frac{[A] \cdot V \cdot (nF)}{Q}$$

where $[A]$ represents the concentration of analyte as determined by quantitative NMR, V the total volume of solution (typically 600 µL), n the mole ratio of transferred electrons, F the Faraday constant, and Q the total charge passed.

Material Characterization. SEM (FEI, Magellan) was used to observe the electrode surface morphology. Each sample was characterized as-prepared, after electro-pretreatment and after CO_2RR by XRD (Bruker, D8 Advance), which had a Cu Kα radiation wavelength of 0.15406 nm.

FIB was performed using the standard lift-out technique on a dual beam FIB-SEM (FEI, Helios Nanolab Dualbeam) equipped with an OmniProbe micromanipulator to prepare samples for TEM analysis on the cross-section of each electrode. Before FIB milling, an electron-beam-assisted (3 kV) protective carbon layer was firstly deposited on the selected area of the electrode surface, followed by a second layer of electron-beam (3 kV) Pt and a third layer of ion-beam-assisted (30 kV) Pt. The total thickness of coating is ~2 µm. A Gallium ion beam of 30 kV were used to mill and thinning the sample to ~100 nm thick lamella. The prepared lamella was mounted to a copper half-grid, and immediately transferred to glovebox for storage.

TEM imaging and SAED were performed on Cs-corrected electron microscope (FEI, Titan cube 80-300), and EELS mapping on a double Cs-corrected electron microscope (FEI, Titan Cubed Themis Z). HRTEM images were processed using a newly developed method to identify individual Cu grains. Briefly, (i) the image is processed by Fast Fourier transform (FFT); (ii) a reflection in the FFT pattern is selected using a line mask (2 by 20 pixels) for inverse Fourier transform to obtain a calculated image; (iii) the line mask is rotated by 1 degree around the center of the selected reflection, followed by inverse Fourier transform to generate the second image, and this step is sequentially repeated by rotating the line mask along a consistent direction to produce 180 calculated images in total; (iv) the 180 images are merged. In the merged image, Cu grains associated with the selected reflection show sharp and clear edges that can be used to determine the crystal facets. The same operations can be applied to different reflections as needed. More detailed theoretical basis and operation procedures of this method will be disclosed in a separate publication shortly.

The high-resolution XPS measurements were carried out using a Kratos Axis ultra DLD spectrometer equipped with a monochromatic Al Kα X-ray source ($h\nu$ = 1486.6 eV) operating at 150 W, a multi-channel plate and delay line detector under a vacuum of ~ 10^{-9} mbar. The high-resolution spectra were collected at fixed analyzer pass energy of 20 eV.

ASSOCIATED CONTENT

Supporting Information

The Supporting Information is available free of charge on the ACS Publications website.

XPS of HQ-Cu; CO_2RR product distributions; EELS spectra; indexed XRD pattern of HQ-Cu after 1 h of CO_2RR; EELS mapping and TEM characterization for PAN-Cu; cathodic current recorded during the electro-reduction pretreatment; FE and current density comparison between electropolished Cu with and without pretreatment; HRTEM image and the corresponding crystal isolation analysis for the oxide-derived layer in HQ-Cu after 1 h of CO_2RR; SEM and TEM characterization for HQ-Cu before and after crystal fragmentation; ECSA analysis.

AUTHOR INFORMATION

Corresponding Author

* yu.han@kaust.edu.sa

Author Contributions

¶Q.L. and H.Z. contributed equally to this work.

Notes

The authors declare no competing financial interest.

ACKNOWLEDGMENT

The financial support for this work was provided by Baseline Funds (BAS/1/1372-01-01) to Y.H. from King Abdullah University of Science and Technology. This research used resources of the Core Labs of King Abdullah University of Science and Technology.

REFERENCES

(1) Bushuyev, O. S.; De Luna, P.; Dinh, C. T.; Tao, L.; Saur, G.; van de Lagemaat, J.; Kelley, S. O.; Sargent, E. H. What Should We Make with CO_2 and How Can We Make It? *Joule* **2018,** *2*, 825-832.
(2) Zhu, D. D.; Liu, J. L.; Qiao, S. Z. Recent Advances in Inorganic Heterogeneous Electrocatalysts for Reduction of Carbon Dioxide. *Adv. Mater.* **2016,** *28*, 3423-3452.
(3) Zheng, T. T.; Jiang, K.; Wang, H. T. Recent Advances in Electrochemical CO_2-to-CO Conversion on Heterogeneous Catalysts. *Adv. Mater.* **2018,** *30*, 1802066.
(4) Gao, D. F.; Aran-Ais, R. M.; Jeon, H. S.; Cuenya, B. R. Rational catalyst and electrolyte design for CO_2 electroreduction towards multicarbon products. *Nat. Catal.* **2019,** *2*, 198-210.

(5) Raciti, D.; Wang, C. Recent Advances in CO_2 Reduction Electrocatalysis on Copper. *ACS Energy Lett.* **2018,** *3*, 1545-1556.
(6) Birhanu, M. K.; Tsai, M. C.; Kahsay, A. W.; Chen, C. T.; Zeleke, T. S.; Ibrahim, K. B.; Huang, C. J.; Su, W. N.; Hwang, B. J. Copper and Copper-Based Bimetallic Catalysts for Carbon Dioxide Electroreduction. *Adv. Mater. Interfaces* **2018,** *5*, 1800919.
(7) Ross, M. B.; De Luna, P.; Li, Y. F.; Dinh, C. T.; Kim, D.; Yang, P.; Sargent, E. H. Designing materials for electrochemical carbon dioxide recycling. *Nat. Catal.* **2019,** *2*, 648-658.
(8) Zheng, X. L.; Ji, Y. F.; Tang, J.; Wang, J. Y.; Liu, B. F.; Steinruck, H. G.; Lim, K.; Li, Y. Z.; Toney, M. F.; Chan, K.; Cui, Y. Theory-guided Sn/Cu alloying for efficient CO_2 electroreduction at low overpotentials. *Nat. Catal.* **2019,** *2*, 55-61.
(9) Lum, Y.; Ager, J. W. Evidence for product-specific active sites on oxide-derived Cu catalysts for electrochemical CO_2 reduction. *Nat. Catal.* **2019,** *2*, 86-93.
(10) Zhuang, T. T.; Liang, Z. Q.; Seifitokaldani, A.; Li, Y.; De Luna, P.; Burdyny, T.; Che, F. L.; Meng, F.; Min, Y. M.; Quintero-Bermudez, R.; Dinh, C. T.; Pang, Y. J.; Zhong, M.; Zhang, B.; Li, J.; Chen, P. N.; Liang, H. Y.; Ge, W. N.; Ye, B. J.; Sinton, D.; Yu, S. H.; Sargent, E. H. Steering post-C-C coupling selectivity enables high efficiency electroreduction of carbon dioxide to multi-carbon alcohols. *Nat. Catal.* **2018,** *1*, 421-428.
(11) Yang, F.; Song, P.; Liu, X. Z.; Mei, B. B.; Xing, W.; Jiang, Z.; Gu, L.; Xu, W. L. Highly Efficient CO_2 Electroreduction on ZnN_4-based Single-Atom Catalyst. *Angew. Chem. Int. Ed.* **2018,** *57*, 12303-12307.
(12) Wang, Y. R.; Huang, Q.; He, C. T.; Chen, Y. F.; Liu, J.; Shen, F. C.; Lan, Y. Q. Oriented electron transmission in polyoxometalate-metalloporphyrin organic framework for highly selective electroreduction of CO_2. *Nat. Commun.* **2018,** *9*, 4466.
(13) Tomisaki, M.; Kasahara, S.; Natsui, K.; Ikemiya, N.; Einaga, Y. Switchable Product Selectivity in the Electrochemical Reduction of Carbon Dioxide Using Boron-Doped Diamond Electrodes. *J. Am. Chem. Soc.* **2019,** *141*, 7414-7420.
(14) Diercks, C. S.; Liu, Y.; Cordova, K. E.; Yaghi, O. M. The role of reticular chemistry in the design of CO_2 reduction catalysts. *Nat. Mater.* **2018,** *17*, 301-307.
(15) Lin, S.; Diercks, C. S.; Zhang, Y. B.; Kornienko, N.; Nichols, E. M.; Zhao, Y. B.; Paris, A. R.; Kim, D.; Yang, P.; Yaghi, O. M.; Chang, C. J. Covalent organic frameworks comprising cobalt porphyrins for catalytic CO_2 reduction in water. *Science* **2015,** *349*, 1208-1213.
(16) Xie, C. L.; Chen, C.; Yu, Y.; Su, J.; Li, Y. F.; Somorjai, G. A.; Yang, P. D. Tandem Catalysis for CO_2 Hydrogenation to C_2-C_4 Hydrocarbons. *Nano Lett.* **2017,** *17*, 3798-3802.
(17) Vasileff, A.; Xu, C. C.; Jiao, Y.; Zheng, Y.; Qiao, S. Z. Surface and Interface Engineering in Copper-Based Bimetallic Materials for Selective CO_2 Electroreduction. *Chem* **2018,** *4*, 1809-1831.
(18) Kim, D.; Kley, C. S.; Li, Y. F.; Yang, P. D. Copper nanoparticle ensembles for selective electroreduction of CO_2 to C_2-C_3 products. *Proc. Natl. Acad. Sci. U. S. A.* **2017,** *114*, 10560-10565.
(19) Mistry, H.; Varela, A. S.; Kuhl, S.; Strasser, P.; Cuenya, B. R. Nanostructured electrocatalysts with tunable activity and selectivity. *Nat. Rev. Mater.* **2016,** *1*, 16009.
(20) Kuhl, K. P.; Cave, E. R.; Abram, D. N.; Jaramillo, T. F. New insights into the electrochemical reduction of carbon dioxide on metallic copper surfaces. *Energ. Environ. Sci.* **2012,** *5*, 7050-7059.
(21) Weng, Z.; Zhang, X.; Wu, Y. S.; Huo, S. J.; Jiang, J. B.; Liu, W.; He, G. J.; Liang, Y. Y.; Wang, H. L. Self-Cleaning Catalyst Electrodes for Stabilized CO_2 Reduction to Hydrocarbons. *Angew. Chem. Int. Ed.* **2017,** *56*, 13135-13139.
(22) Hahn, C.; Hatsukade, T.; Kim, Y. G.; Vailionis, A.; Baricuatro, J. H.; Higgins, D. C.; Nitopi, S. A.; Soriaga, M. P.; Jaramillo, T. F. Engineering Cu surfaces for the electrocatalytic conversion of CO_2: Controlling selectivity toward oxygenates and hydrocarbons. *Proc. Natl. Acad. Sci. U. S. A.* **2017,** *114*, 5918-5923.
(23) Hori, Y.; Takahashi, I.; Koga, O.; Hoshi, N. Selective formation of C_2 compounds from electrochemical reduction of CO_2 at a series of copper single crystal electrodes. *J. Phys. Chem. B* **2002,** *106*, 15-17.
(24) Hori, Y.; Wakebe, H.; Tsukamoto, T.; Koga, O. Adsorption of CO Accompanied with Simultaneous Charge-Transfer on Copper Single-Crystal Electrodes Related with Electrochemical Reduction of CO_2 to Hydrocarbons. *Surf. Sci.* **1995,** *335*, 258-263.
(25) Luo, W. J.; Nie, X. W.; Janik, M. J.; Asthagiri, A. Facet Dependence of CO_2 Reduction Paths on Cu Electrodes. *ACS Catal.* **2016,** *6*, 219-229.
(26) Wu, Y. A.; McNulty, I.; Liu, C.; Lau, K. C.; Liu, Q.; Paulikas, A. P.; Sun, C.-J.; Cai, Z.; Guest, J. R.; Ren, Y.; Stamenkovic, V.; Curtiss, L. A.; Liu, Y.; Rajh, T. Facet-dependent active sites of a single Cu_2O particle photocatalyst for CO_2 reduction to methanol. *Nat. Energy* **2019,** *4*, 957-968.
(27) Shaw, S. K.; Berna, A.; Feliu, J. M.; Nichols, R. J.; Jacob, T.; Schiffrin, D. J. Role of axially coordinated surface sites for electrochemically controlled carbon monoxide adsorption on single crystal copper electrodes. *Phys. Chem. Chem. Phys.* **2011,** *13*, 5242-5251.
(28) Lv, J. J.; Jouny, M.; Luc, W.; Zhu, W. L.; Zhu, J. J.; Jiao, F. A Highly Porous Copper Electrocatalyst for Carbon Dioxide Reduction. *Adv. Mater.* **2018,** *30*, 1803111.
(29) Suen, N. T.; Kong, Z. R.; Hsu, C. S.; Chen, H. C.; Tung, C. W.; Lu, Y. R.; Dong, C. L.; Shen, C. C.; Chung, J. C.; Chen, H. M. Morphology Manipulation of Copper Nanocrystals and Product Selectivity in the Electrocatalytic Reduction of Carbon Dioxide. *ACS Catal.* **2019,** *9*, 5217-5222.
(30) Wang, L.; Nitopi, S.; Wong, A. B.; Snider, J. L.; Nielander, A. C.; Morales-Guio, C. G.; Orazov, M.; Higgins, D. C.; Hahn, C.; Jaramillo, T. F. Electrochemically converting carbon monoxide to liquid fuels by directing selectivity with electrode surface area. *Nat. Catal.* **2019,** *2*, 702-708.
(31) Wang, Y. F.; Chen, Z.; Han, P.; Du, Y. H.; Gu, Z. X.; Xu, X.; Zheng, G. F. Single-Atomic Cu with Multiple Oxygen Vacancies on Ceria for Electrocatalytic CO_2 Reduction to CH_4. *ACS Catal.* **2018,** *8*, 7113-7119.
(32) Ma, S.; Sadakiyo, M.; Heima, M.; Luo, R.; Haasch, R. T.; Gold, J. I.; Yamauchi, M.; Kenis, P. J. A. Electroreduction of Carbon Dioxide to Hydrocarbons Using Bimetallic Cu-Pd Catalysts with Different Mixing Patterns. *J. Am. Chem. Soc.* **2017,** *139*, 47-50.
(33) Lu, L.; Sun, X. F.; Ma, J.; Yang, D. X.; Wu, H. H.; Zhang, B. X.; Zhang, J. L.; Han, B. X. Highly Efficient Electroreduction of CO_2 to Methanol on Palladium-Copper Bimetallic Aerogels. *Angew. Chem. Int. Ed.* **2018,** *57*, 14149-14153.
(34) Lee, S. Y.; Jung, H.; Kim, N. K.; Oh, H. S.; Min, B. K.; Hwang, Y. J. Mixed Copper States in Anodized Cu Electrocatalyst for Stable and Selective Ethylene Production from CO_2 Reduction. *J. Am. Chem. Soc.* **2018,** *140*, 8681-8689.
(35) Jung, H.; Lee, S. Y.; Lee, C. W.; Cho, M. K.; Won, D. H.; Kim, C.; Oh, H. S.; Min, B. K.; Hwang, Y. J. Electrochemical Fragmentation of Cu_2O Nanoparticles Enhancing Selective C-C Coupling from CO_2 Reduction Reaction. *J. Am. Chem. Soc.* **2019,** *141*, 4624-4633.
(36) Mistry, H.; Varela, A. S.; Bonifacio, C. S.; Zegkinoglou, I.; Sinev, I.; Choi, Y. W.; Kisslinger, K.; Stach, E. A.; Yang, J. C.; Strasser, P.; Cuenya, B. R. Highly selective plasma-activated copper catalysts for carbon dioxide reduction to ethylene. *Nat. Commun.* **2016,** *7*, 12123.
(37) Scott, S. B.; Hogg, T. V.; Landers, A. T.; Maagaard, T.; Bertheussen, E.; Lin, J. C.; Davis, R. C.; Beeman, J. W.; Higgins, D.; Drisdell, W. S.; Hahn, C.; Mehta, A.; Seger, B.; Jaramillo, T. F.; Chorkendorff, I. Absence of Oxidized Phases in Cu under CO Reduction Conditions. *ACS Energy Lett.* **2019,** *4*, 803-804.
(38) Jiang, K.; Sandberg, R. B.; Akey, A. J.; Liu, X. Y.; Bell, D. C.; Norskov, J. K.; Chan, K. R.; Wang, H. T. Metal ion cycling of Cu

foil for selective C-C coupling in electrochemical CO_2 reduction. *Nat. Catal.* **2018,** *1*, 111-119.
(39) Kim, T.; Kargar, A.; Luo, Y.; Mohammed, R.; Martinez-Loran, E.; Ganapathi, A.; Shah, P.; Fenning, D. P. Enhancing C_2–C_3 Production from CO_2 on Copper Electrocatalysts via a Potential-Dependent Mesostructure. *ACS Appl. Energy Mater.* **2018,** *1*, 1965-1972.
(40) Gu, Z.; Yang, N.; Han, P.; Kuang, M.; Mei, B.; Jiang, Z.; Zhong, J.; Li, L.; Zheng, G. Oxygen Vacancy Tuning toward Efficient Electrocatalytic CO_2 Reduction to C_2H_4. *Small Methods* **2019,** *3*, 1800449.
(41) Zhu, Q.; Sun, X.; Yang, D.; Ma, J.; Kang, X.; Zheng, L.; Zhang, J.; Wu, Z.; Han, B. Carbon dioxide electroreduction to C_2 products over copper-cuprous oxide derived from electrosynthesized copper complex. *Nat. Commun.* **2019,** *10*, 3851.
(42) Cavalca, F.; Ferragut, R.; Aghion, S.; Eilert, A.; Diaz-Morales, O.; Liu, C.; Koh, A. L.; Hansen, T. W.; Pettersson, L. G. M.; Nilsson, A. Nature and Distribution of Stable Subsurface Oxygen in Copper Electrodes During Electrochemical CO_2 Reduction. *J. Phys. Chem. C* **2017,** *121*, 25003-25009.
(43) Eilert, A.; Cavalca, F.; Roberts, F. S.; Osterwalder, J.; Liu, C.; Favaro, M.; Crumlin, E. J.; Ogasawara, H.; Friebel, D.; Pettersson, L. G. M.; Nilsson, A. Subsurface Oxygen in Oxide-Derived Copper Electrocatalysts for Carbon Dioxide Reduction. *J. Phys. Chem. Lett.* **2017,** *8*, 285-290.
(44) Dutta, A.; Rahaman, M.; Luedi, N. C.; Broekmann, P. Morphology Matters: Tuning the Product Distribution of CO_2 Electroreduction on Oxide-Derived Cu Foam Catalysts. *ACS Catal.* **2016,** *6*, 3804-3814.
(45) Handoko, A. D.; Ong, C. W.; Huang, Y.; Lee, Z. G.; Lin, L. Y.; Panetti, G. B.; Yeo, B. S. Mechanistic Insights into the Selective Electroreduction of Carbon Dioxide to Ethylene on Cu_2O-Derived Copper Catalysts. *J. Phys. Chem. C* **2016,** *120*, 20058-20067.
(46) Kas, R.; Kortlever, R.; Milbrat, A.; Koper, M. T. M.; Mul, G.; Baltrusaitis, J. Electrochemical CO_2 reduction on Cu_2O-derived copper nanoparticles: controlling the catalytic selectivity of hydrocarbons. *Phys. Chem. Chem. Phys.* **2014,** *16*, 12194-12201.
(47) Ren, D.; Deng, Y. L.; Handoko, A. D.; Chen, C. S.; Malkhandi, S.; Yeo, B. S. Selective Electrochemical Reduction of Carbon Dioxide to Ethylene and Ethanol on Copper(I) Oxide Catalysts. *ACS Catal.* **2015,** *5*, 2814-2821.
(48) Huang, Y.; Handoko, A. D.; Hirunsit, P.; Yeo, B. S. Electrochemical Reduction of CO_2 Using Copper Single-Crystal Surfaces: Effects of CO* Coverage on the Selective Formation of Ethylene. *ACS Catal.* **2017,** *7*, 1749-1756.
(49) Yuan, L.; Wang, Y. Q.; Mema, R.; Zhou, G. W. Driving force and growth mechanism for spontaneous oxide nanowire formation during the thermal oxidation of metals. *Acta Mater.* **2011,** *59*, 2491-2500.
(50) Zhu, Y. F.; Mimura, K.; Isshiki, M. Oxidation mechanism of copper at 623-1073 K. *Mater. Trans.* **2002,** *43*, 2173-2176.
(51) Keast, V. J.; Scott, A. J.; Brydson, R.; Williams, D. B.; Bruley, J. Electron energy-loss near-edge structure – a tool for the investigation of electronic structure on the nanometre scale. *J. Microsc.* **2001,** *203*, 135-175.
(52) Li, C. W.; Kanan, M. W. CO_2 Reduction at Low Overpotential on Cu Electrodes Resulting from the Reduction of Thick Cu_2O Films. *J. Am. Chem. Soc.* **2012,** *134*, 7231-7234.
(53) Wang, Y. X.; Raciti, D.; Wang, C. High-Flux CO Reduction Enabled by Three-Dimensional Nanostructured Copper Electrodes. *ACS Catal.* **2018,** *8*, 5657-5663.
(54) Eilert, A.; Roberts, F. S.; Friebel, D.; Nilsson, A. Formation of Copper Catalysts for CO_2 Reduction with High Ethylene/Methane Product Ratio Investigated with In Situ X-ray Absorption Spectroscopy. *J. Phys. Chem. Lett.* **2016,** *7*, 1466-1470.
(55) Mandal, L.; Yang, K. R.; Motapothula, M. R.; Ren, D.; Lobaccaro, P.; Patra, A.; Sherburne, M.; Batista, V. S.; Yeo, B. S.; Ager, J. W.; Martin, J.; Venkatesan, T. Investigating the Role of Copper Oxide in Electrochemical CO_2 Reduction in Real Time. *ACS Appl. Mater. Interfaces* **2018,** *10*, 8574-8584.
(56) Verdaguer-Casadevall, A.; Li, C. W.; Johansson, T. P.; Scott, S. B.; McKeown, J. T.; Kumar, M.; Stephens, I. E. L.; Kanan, M. W.; Chorkendorff, I. Probing the Active Surface Sites for CO Reduction on Oxide-Derived Copper Electrocatalysts. *J. Am. Chem. Soc.* **2015,** *137*, 9808-9811.
(57) Li, C. W.; Ciston, J.; Kanan, M. W. Electroreduction of carbon monoxide to liquid fuel on oxide-derived nanocrystalline copper. *Nature* **2014,** *508*, 504.
(58) Mariano, R. G.; McKelvey, K.; White, H. S.; Kanan, M. W. Selective increase in CO_2 electroreduction activity at grain-boundary surface terminations. *Science* **2017,** *358*, 1187-1192.
(59) Pang, Y.; Li, J.; Wang, Z.; Tan, C.-S.; Hsieh, P.-L.; Zhuang, T.-T.; Liang, Z.-Q.; Zou, C.; Wang, X.; De Luna, P.; Edwards, J. P.; Xu, Y.; Li, F.; Dinh, C.-T.; Zhong, M.; Lou, Y.; Wu, D.; Chen, L.-J.; Sargent, E. H.; Sinton, D. Efficient electrocatalytic conversion of carbon monoxide to propanol using fragmented copper. *Nat. Catal.* **2019,** *2*, 251-258.
(60) Feng, X. F.; Jiang, K. L.; Fan, S. S.; Kanan, M. W. A Direct Grain-Boundary-Activity Correlation for CO Electroreduction on Cu Nanoparticles. *Acs Central Sci* **2016,** *2*, 169-174.
(61) Feng, X.; Jiang, K.; Fan, S.; Kanan, M. W. Grain-Boundary-Dependent CO_2 Electroreduction Activity. *J. Am. Chem. Soc.* **2015,** *137*, 4606-4609.

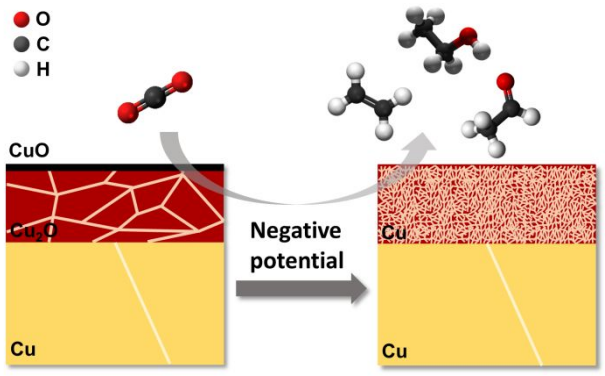
O
C
H
CuO
Cu_2O
Cu
Negative potential
Cu
Cu